Journal of Computational and Applied Mathematics 264 (2014) 131–138

Contents lists available at ScienceDirect

Journal of Computational and Applied Mathematics

journal homepage: www.elsevier.com/locate/cam

Elastic analysis of a circumferential crack in an isotropic curved beam using the modified mapping–collocation method

Aydin Amireghbali [a], Demirkan Coker [a,b,*]

[a] Department of Aerospace Eng., Middle East Technical University, Ankara, Turkey
[b] METU Center for Wind Energy (METUWIND), Ankara, Turkey

ARTICLE INFO

Article history:
Received 13 February 2013
Received in revised form 24 December 2013

Keywords:
Modified mapping–collocation (MMC) method
Linear elastic fracture mechanics (LEFM)
Stress intensity factor (SIF)
Circumferential crack
Curved beam
Complex analysis

ABSTRACT

The modified mapping-collocation (MMC) method was applied to the boundary value problem (BVP) of a circumferential crack in an isotropic elastic curved beam subjected to pure bending moment loading. The stress correlation technique is then used to determine opening and sliding mode stress intensity factor (SIF) values based on the computed stress field near the crack tip. The MMC method aims at solving two-dimensional BVP of linear elastic fracture mechanics (LEFM) circumventing the need for direct treatment of the biharmonic equation by combining the power of analytic tools of complex analysis (Muskhelishvili formulation, conformal mapping, and continuation arguments) with simplicity of applying the boundary collocation method as a numerical solution approach. A good qualitative agreement between the computed stress contours and the fringe shapes obtained from the photoelastic experiment on a plexiglass specimen is observed. A quantitative comparison with FEM results is also made using ANSYS. The effect of crack size, crack position and beam thickness variation on SIF values and mode-mixity is investigated.

1. Introduction

In metal components with a curved geometry, cracks initiate in the radial direction. However, in heterogeneous structures such as curved laminated composites, cracks occur circumferentially [1]. Even though significant amount of work has been carried out on radial cracks in the literature, sufficient attention has not been paid to the analysis of circumferential cracks. In contrast to radial cracks, the curved crack geometry, independent of applied loading, leads to mixed-mode fracture consisting of opening mode (mode-I) and sliding mode (mode-II).

The modified mapping–collocation (MMC) method [2] was introduced in 1970 to treat two-dimensional fracture mechanics problems for isotropic problems and later developed further for orthotropic cases [3]. In the 1970s the method was applied to a range of two-dimensional problems, all with radial (and therefore straight) cracks; a radial crack in a circular ring [4], a radial crack in a segment of a circular ring [5] and radial cracks emanating from both the inner and outer surfaces of a circular ring [6]. In all these cases mode-I fracture of radial cracks were investigated.

In the present study, the MMC method is applied in order to compute the stress field in an isotropic curved beam with a circumferential crack subjected to pure bending moment (Fig. 1). Thereafter, the stress correlation [7] technique is incorporated in the MMC method to calculate the SIF values for both the opening and sliding modes from the stresses

* Corresponding author at: Department of Aerospace Eng., Middle East Technical University, Ankara, Turkey. Tel.: +90 3122104253; fax: +90 3122104250.
E-mail addresses: aydin.amireghbali@gmail.com (A. Amireghbali), coker@metu.edu.tr, demir.coker@gmail.com (D. Coker).

0377-0427/$ – see front matter © 2014 Elsevier B.V. All rights reserved.
http://dx.doi.org/10.1016/j.cam.2013.12.053

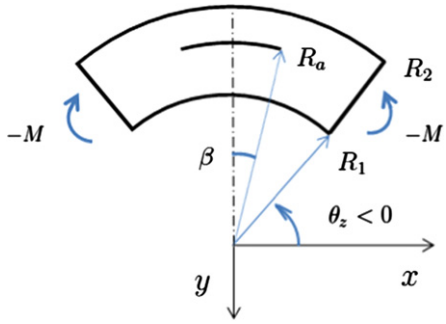

Fig. 1. Curved beam with circumferential crack.

obtained at the vicinity of the crack tip. A parametric study of the effect of crack size, crack position and beam thickness on SIFs and their fraction (mode-mixity) is presented.

2. Theory

The analytic basis of the MMC method is mainly the comprehensive work of N.I. Muskhelishvili [8], in which his complex representations for boundary condition equations besides conformal mapping and continuation (or extension) arguments of both Muskhelishvili and Kartzivadze are introduced and applied to various two-dimensional linear elastic fracture mechanics (LEFM) problems. The numerical part uses the boundary collocation method to solve the overdetermined linear system of equations supplied by the analytic part in a least-square sense.

2.1. Muskhelishvili's complex formulation

According to G.V. Kolosov's formulation [8], only two complex analytic functions (e.g. $\phi(z)$ and $\psi(z)$) are needed in order to describe the stress field in a two-dimensional elastic body:

$$\sigma_y + \sigma_x = 4\Re\{\phi'(z)\} \tag{1}$$

$$\sigma_y - \sigma_x + 2i\sigma_{xy} = 2[\bar{z}\phi''(z) + \psi'(z)]. \tag{2}$$

Further, Muskhelishvili [8] states the boundary condition equations in terms of $\phi(z)$ and $\psi(z)$. His complex formulation for the stress boundary condition equations is:

$$N - iT = \phi'(z) + \overline{\phi'(z)} - [\bar{z}\phi''(z) + \psi'(z)]e^{2i\theta} \tag{3}$$

where N is the normal stress component of boundary traction and T is the tangential component. Also the local force boundary condition equation is given [8] by:

$$(F_x + iF_y)_{on\ AB} = b.i[\phi(z) + z\overline{\phi'(z)} + \overline{\psi(z)}]_{z_A}^{z_B} \tag{4}$$

where F_x and F_y are the local force vector components on segment AB on the boundary and b is the beam depth in the direction perpendicular to the complex z-plane. However A and B do not refer to any particular point on the boundary, once point A is selected on the boundary, point B is chosen such that when *moving* from A to B, the body appears on the left side of the segment AB.

The real power of complex analysis approach to the problem appears when investigating cracked bodies. Finding a proper function which maps the image plane (ζ-plane) into physical plane (z-plane) provides the opportunity of applying the theorems and tools of complex analysis.

2.2. Laurent theorem and series

According to the Laurent theorem, for any function (e.g. $\phi(\zeta)$) that is analytic on an annulus **R**, centered at $\zeta = 0$, there exists a unique power series expansion of the form:

$$\phi(\zeta) = \sum_{n=-\infty}^{+\infty} a_n \zeta^n \tag{5}$$

(namely a Laurent series) which converges to that function on the region **R**.

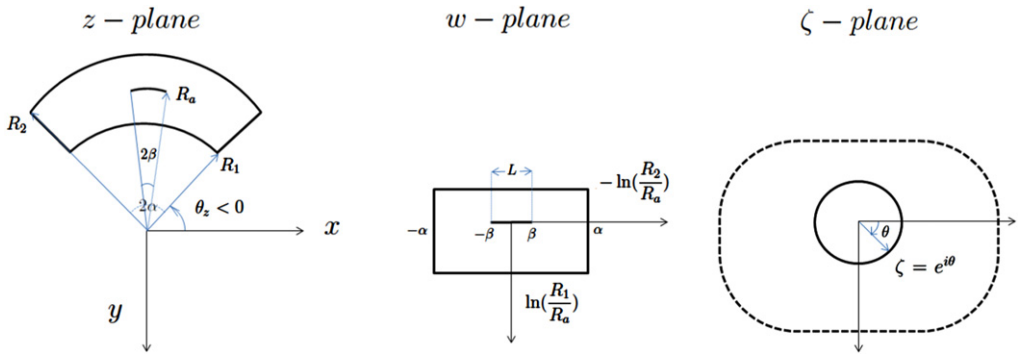

Fig. 2. The successive mapping plan.

Although in the case of cracked curved beam, the outer mapped boundary (i.e. image of the curved beam in the ζ-plane) is not circular (Fig. 2), there is no a priori reason to suspect that the region of convergence of the series could not be extended over to it (i.e. the outer non-circular boundary of the punctured region in the ζ-plane). Hence, it seems still possible to approximate the $\phi(\zeta)$ by a truncated Laurent series on the region. Taking into account the stress symmetry (mirror) with respect to the imaginary axis, the series form is modified to:

$$\phi(\zeta) = \sum_{n=-M}^{N} [iA_{2n}\zeta^{2n} + A_{2n+1}\zeta^{2n+1}] \tag{6}$$

where A_{2n} and A_{2n+1} are purely real coefficients and M and N are non-negative integers. It can be shown that the proposed series form intrinsically induces analytic satisfaction of the zero shear stress and zero horizontal displacement conditions on the symmetry (imaginary) axis.

2.3. The mapping function

In order to map the unit circle in the image plane to a circumferential crack in the physical plane, one may combine two successive mappings into one composite function $z = h(\zeta)$:

$$z = f(g(\zeta)) = h(\zeta) = R_a \exp\left\{i\left[\frac{\beta}{2}(\zeta + \zeta^{-1}) - \frac{\pi}{2}\right]\right\} \tag{7}$$

where the function mapping the unit circle in ζ-plane into w-plane is:

$$w = g(\zeta) = \frac{L}{4}(\zeta + \zeta^{-1}) \tag{8}$$

(note that $L = 2\beta$) and the function mapping w-plane into the z-plane is:

$$z = f(w) = R_a \exp\left\{i\left(w - \frac{\pi}{2}\right)\right\} \tag{9}$$

and R_a and β are geometrical parameters as shown in Fig. 2.

2.4. The continuation argument

In close relation to application of conformal mapping to cracked body problems, the concept of analytic continuation was developed and applied by I.N. Kartzivadze (for the unit circle) and later by N.I. Muskhelishvili (for the real axis) [8].

Forcing the function $\phi(\zeta)$ to *continue* across into the unit circle interior by defining:

$$\phi(\zeta) = -\frac{h(\zeta)}{\overline{h'}\left(\frac{1}{\zeta}\right)}\overline{\phi'}\left(\frac{1}{\zeta}\right) - \overline{\psi}\left(\frac{1}{\zeta}\right), \quad |\zeta| < 1 \tag{10}$$

which is called Kartzivadze's continuation (or extension) argument. The bar-notation for any complex analytic function F implies:

$$\overline{F}\left(\frac{1}{\zeta}\right) = \overline{F\left(\frac{1}{\overline{\zeta}}\right)}. \tag{11}$$

Consequently [8];

$$\psi(\zeta) = -\overline{\phi}\left(\frac{1}{\zeta}\right) - \frac{\overline{h}\left(\frac{1}{\zeta}\right)}{h'(\zeta)}\phi'(\zeta), \quad |\zeta| > 1. \tag{12}$$

This result is of extreme importance from two aspects; firstly expressing $\psi(\zeta)$ in terms of $\phi(\zeta)$ reduces number of the *complex potentials* needed to describe the stress field to one (i.e. solely $\phi(\zeta)$), and secondly it analytically satisfies traction-free conditions on the crack boundary (i.e. the unit circle) by making the left hand side expression in the force boundary conditions zero (see Eq. (13)).

3. Implementation

Transferring boundary condition equations into the image plane (ζ-plane), where they are to be solved, causes the mapping function and its derivatives (via the chain rule) to enter into the formulations. The local force boundary condition equation is found to be [8]:

$$b.i\left[\phi(\zeta) - \phi\left(\frac{1}{\overline{\zeta}}\right) + \left(h(\zeta) - h\left(\frac{1}{\overline{\zeta}}\right)\right)\overline{\frac{\phi'(\zeta)}{h'(\zeta)}}\right]_{\zeta_A}^{\zeta_B} = (F_x + iF_y)_{on\ \overline{AB}}. \tag{13}$$

The classical solution for the crack-less curved beam under pure bending, is given by H. Golovin [9]. The right hand side expression in Eq. (13) for moment-exerted boundary could be obtained by integrating Golovin's solution for the normal stress distribution equation as:

$$(F_x + iF_y)_{on\ \overline{AB}} = -(\cos(\alpha) + i\sin(\alpha))\frac{4M}{N_G}\left[R_1^2 r \ln\left(\frac{R_1}{r}\right) + R_2^2 r \ln\left(\frac{r}{R_2}\right) + \frac{R_1^2 R_2^2}{r}\ln\left(\frac{R_2}{R_1}\right)\right]_{r_A}^{r_B} \tag{14}$$

where α stands for the half arc beam angle (and in this study is equal to $\frac{\pi}{4}$), M is the applied moment's absolute value and:

$$N_G = (R_2^2 - R_1^2)^2 - 4R_1^2R_2^2\left(\ln\left(\frac{R_2}{R_1}\right)\right)^2. \tag{15}$$

On the other two (upper and lower) boundaries, right hand side of Eq. (13) is obviously zero, since there is no traction.

Substituting expressions according to the $\phi(\zeta)$ expansion (6) into the boundary condition equation (13), one may obtain two linear equations at the mid-point between each two successive points A and B on the boundary, whose unknowns are the coefficients of the Laurent series. These mid-points are called stations. It can be seen from Eq. (13) that on the unit circle (crack image), since $\zeta = \frac{1}{\overline{\zeta}}$, the left hand side becomes zero, satisfying the traction-free condition automatically.

The overdetermined system of linear (boundary condition) equations is constructed by writing the local force equations for stations on the boundary. Note that since the *stress symmetry* is held automatically by Eq. (6), only half of the beam is considered in the computations. The stations are placed in equal distances to each other, but not at the corners (common points of the boundaries). For all of the cases, the lower, the moment-exerted and the upper boundaries have 3, 4 and 5 stations, respectively. Number of the equations is found to be $2*(3+4+5) = 24$. For the series expansion, M and N values both were set to 3. Number of the unknowns can be calculated from $2*(M+N)+1$ as 13, which means the series has 13 terms (and therefore coefficients). Hence the *redundancy factor* of the overdetermined system of equations (defined as number of equations divided by number of unknowns) is $\simeq 2$. The highest degree of the polynomial given by the expansion is 7 and the lowest is -6. The system is solved in a least square sense and the solution determines the series expansion coefficients for the Muskhelishvili potential $\phi(\zeta)$. Then the stress at each point of the body is found using Kolosov's formulae (1) and (2) in the image region:

$$\sigma_y + \sigma_x = 4\Re\left\{\frac{\phi'(\zeta)}{h'(\zeta)}\right\} \tag{16}$$

$$\sigma_y - \sigma_x + 2i\sigma_{xy} = 2\left\{\overline{h(\zeta)}\,\frac{h'(\zeta)\phi''(\zeta) - h''(\zeta)\phi'(\zeta)}{[h'(\zeta)]^2} + \psi'(\zeta)\right\}\Big/ h'(\zeta).$$

Finally using the stress correlation technique, SIFs are obtained by extrapolating the stress values in the vicinity ahead of the crack tip considering that:

$$K_{\mathrm{I}} = \lim_{r\to 0}\sqrt{2\pi r}\,\sigma_{22}(r, 0) \tag{17}$$

$$K_{\mathrm{II}} = \lim_{r\to 0}\sqrt{2\pi r}\,\sigma_{12}(r, 0) \tag{18}$$

where I and II represent opening and sliding modes respectively and r stands for local radial distance from the crack tip, and 1 and 2 represent local coordinates tangential and perpendicular to the crack at its tip.

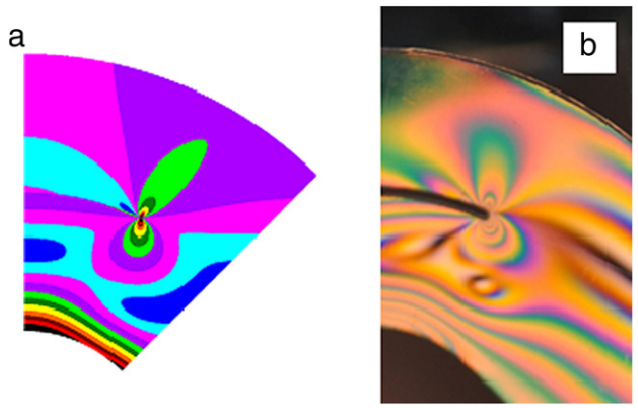

Fig. 3. The maximum shear stress contours for the *sample beam* according to the: (a) MATLAB code applying the MMC method (b) photoelastic test of plexiglass specimen.

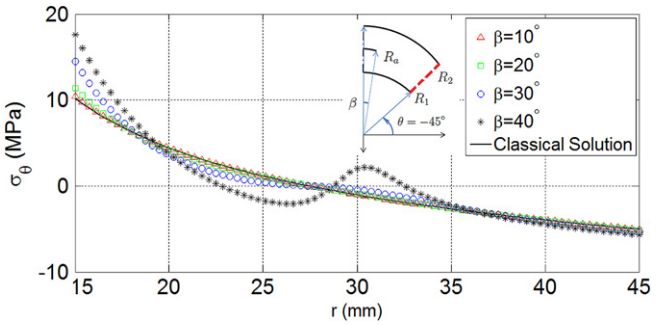

Fig. 4. Deviation from the classical solution for normal stress distribution on the moment-exerted boundary for the *sample beam* with different β values.

4. Results

An opening moment of -10 N m (i.e. $M = 10$ N m in Fig. 1) is applied to ends of the curved beam and a depth, b, of 0.01 m is considered for all of the beams under investigation. Considering the symmetry of the problem with respect to the imaginary axis, the MMC method is applied successfully to one of the halves of the beam in order to find the stress field and thereafter mode-I and mode-II SIFs. Firstly, the calculations are carried out for a *sample beam* of 30 mm thickness ($R_1 = 15$ mm and $R_2 = 45$ mm) containing a crack of 25° half arc angle, β, which is located on its center line ($R_a = 30$ mm). Later the effect of geometrical parameters variation on mode-I SIF and mode-mixity is studied in general.

The maximum shear stress contours for the *sample beam* are shown in Fig. 3(a). The asymmetric contour shape around the crack tip signifies the mixed-mode stress field. Uniformly changing contours near the inner radius imitates the rainbow-shaped fringes predicted by the classical solution i.e. in the absence of a crack [9]. The maximum shear stress contours obtained from photoelastic 4-point bending test of a plexiglass specimen of the same dimensions is shown in Fig. 3(b). Note that a classic 4-point bending test does not lead to application of a *pure* bending moment to the curved part of an L-shaped beam (because of the straight arm shape, and no matter how far the point forces are applied). Having this in mind and considering manufacturing imperfections (especially at the crack tips) and also noting deflection of the test specimen (which is not incorporated in the MMC-generated plot), a good agreement is observed between the numerical and experimental results in terms of the contour shapes.

The *recalculated* stress values on the boundaries give a measure of the accuracy of the solution. In Fig. 4 the obtained normal stress distribution on the moment-exerted boundary is plotted (by the markers) together with the classical (crackless) solution (the solid line) for the *sample beam*. Although the same distribution is expected, a deviation from the classical solution is observed with an increase in the crack half angle (β). The *root mean square (RMS)* values of the deviation for β values 10°, 20°, 30° and 40° are calculated as 0.05, 0.25, 0.96 and 2.19 MPa respectively. Dividing by $\sigma = (\sigma_\theta)_{r=R_1} = 10.19$ MPa, one has 0.5%, 2.5%, 9.4% and 22% as a measure of the deviation from the classical solution. Also it is observed that all of the stress distributions given by the method in Fig. 4, result in nearly the same moment value about the origin (with a maximum of 3.2% deviation from -10 N m at $\beta = 30°$, where for the other cases these values are below 0.5%). Producing a somewhat negligible non-zero force resultant in the circumferential direction, these stress distributions do not produce a *pure* moment. The ratio of these force values to the resultant of the positive σ_θ on the moment-exerted boundary reaches a maximum of 7.6% for $\beta = 40°$. The immediate neighbor is 1.36% for $\beta = 30°$. The boundary conditions are satisfied more accurately for smaller cracks.

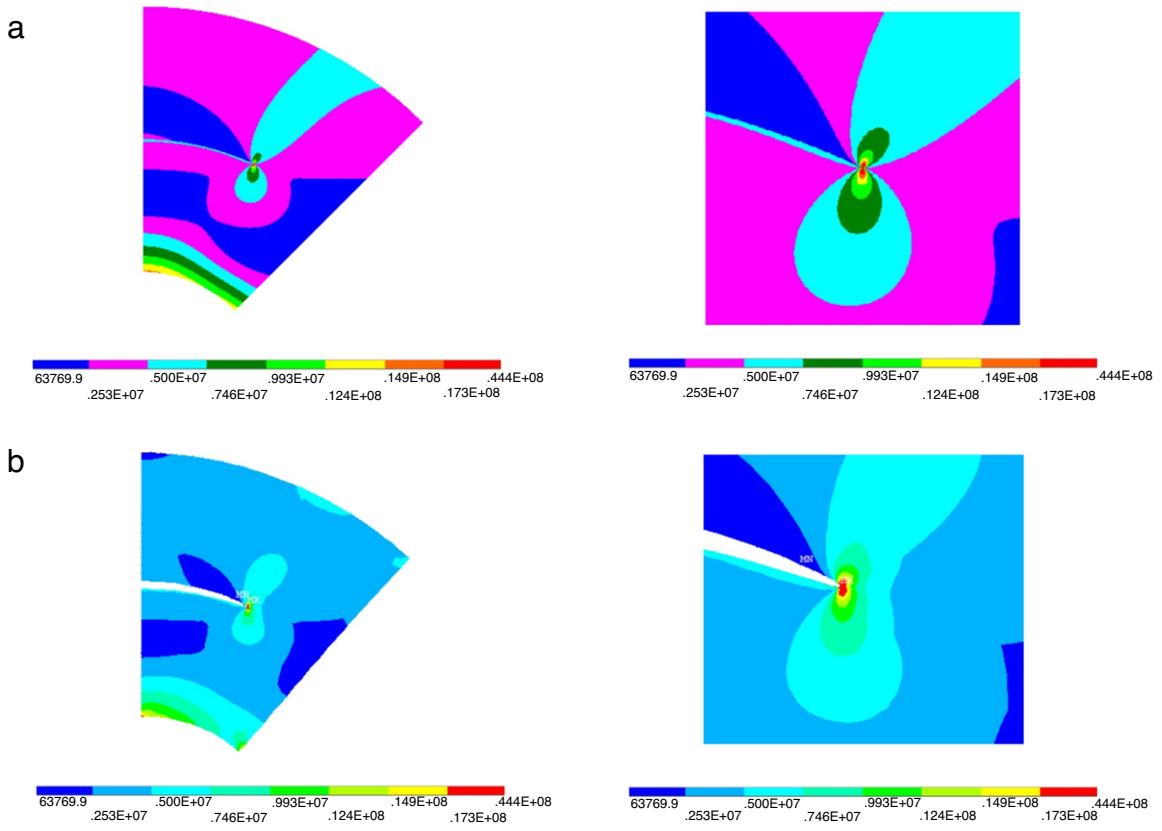

Fig. 5. The contours of $2\tau_{max}$ for the *sample beam* obtained by (a) MMC method and (b) FEM, a closer look ($1\ cm^2$) to the crack tip is provided for each case on the right side.

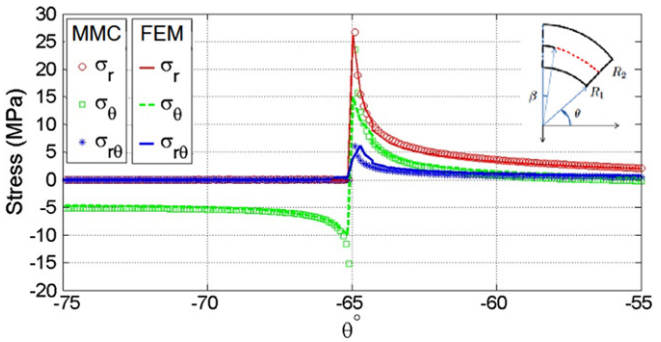

Fig. 6. The stress components on a small arc including the crack tip of the *sample beam* obtained by MMC method and FEM.

A finite element model of the half-*sample beam* was analyzed using ANSYS (Mechanical APDL) to verify the solution quantitatively. *PLANE* 183 elements were selected. The encircling crack tip singular elements have a radius of 0.1 mm. All of the nodes on the axis of symmetry are restricted in the horizontal direction with one of the nodes restricted also in the vertical direction to prevent rigid body motion. The contours of constant $2\tau_{\max}$ are shown in the same contour levels in Fig. 5(a) for the MMC method and in Fig. 5(b) for FEM. A zoomed view of the crack tip for both the MMC method and FEM are presented on the right. The contour shapes indicate a good agreement in terms of stress values. The stress fringes end at the crack tip for both the photoelastic test and the MMC method (Figs. 3(b) and 5(a)); whereas this behavior is not observed for the FEM (Fig. 5(b)).

In Fig. 6, the stress components in polar coordinates are shown on an arc that includes the crack plane for the *sample beam*. The plot indicates $1/\sqrt{r}$ linear-elastic singularity at the crack tip. Note the abnormal jump in the FEM-calculated $\sigma_{r\theta}$ stress component and also its sudden drop right before reaching the crack tip which makes calculation of mode-II SIF values problematic. Except for $\sigma_{r\theta}$, the stresses at the crack tip, the stresses are in good agreement between the MMC and

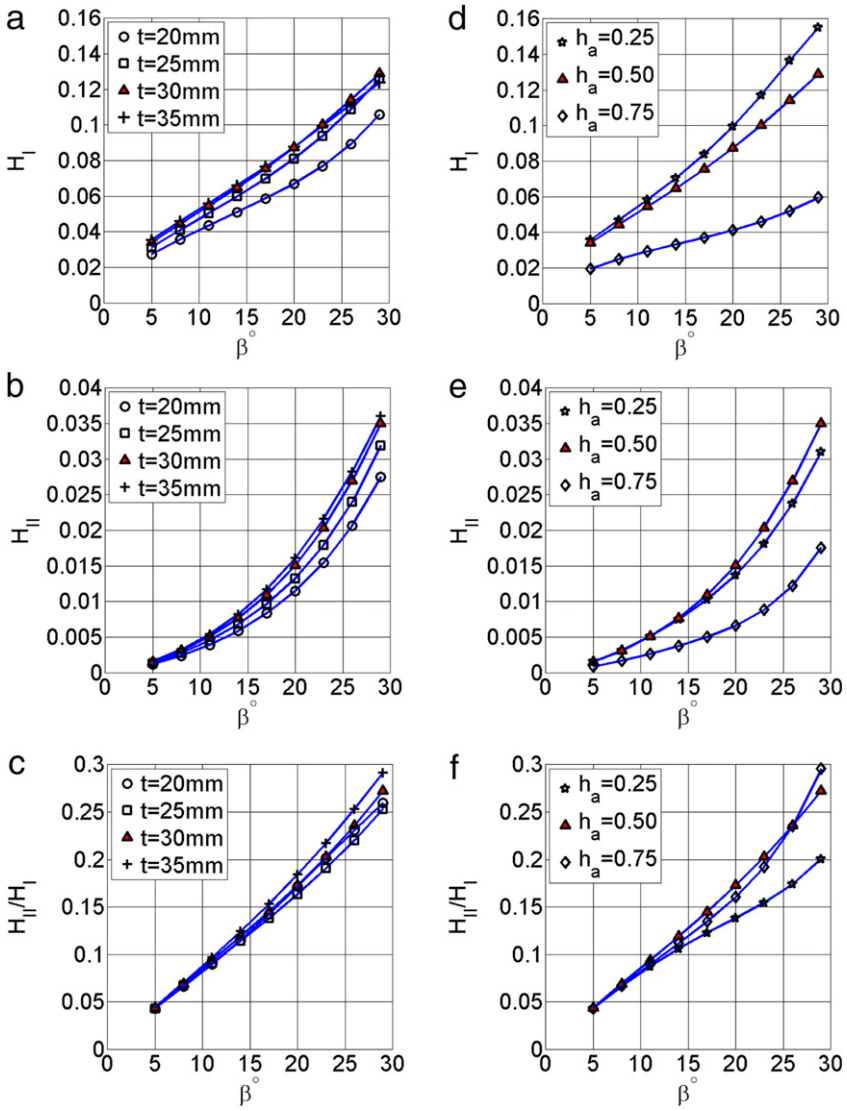

Fig. 7. (a) Non-dimensionalized mode-I SIF, (b) non-dimensionalized mode-II SIF, (c) mode-mixity, versus crack half arc angle, β, for a central crack ($h_a = 0.5$) at $R_a = 30$ mm, in beams of $t = 20, 25, 30$ mm and 35 mm thickness, for which corresponding non-dimensionalizing stress values are $\sigma = (\sigma_\theta)_{r=R_1} = 19.4,\ 13.4,\ 10.2$ and 8.3 MPa respectively (d) non-dimensionalized mode-I SIF, (e) non-dimensionalized mode-II SIF, (f) mode-mixity, versus crack half arc angle, β, for different crack positions $h_a = 0.25, 0.5$ and 0.75 for the beam with $R_1 = 15$ mm and $R_2 = 45$ mm for which the non-dimensionalizing stress value is $\sigma = (\sigma_\theta)_{r=R_1} = 10.2$ MPa.

FE methods. The *traction-free* boundary conditions on the crack surface ($\sigma_r = 0$, $\sigma_{r\theta} = 0$) are satisfied by the MMC method to an order of 10^{-12} MPa (or 10^{-6} Pa).

It is convenient to define a non-dimensionalized SIF parameter, H_i, as:

$$H_i = \frac{K_i}{\sigma\sqrt{2\pi R_m}} \tag{19}$$

where σ is the value of the normal stress value in the classical (crack-less) solution at inner radius of the moment-exerted boundary of the beam, R_m is the center line radius of the beam ($R_m = (R_1 + R_2)/2$); and i stands for either opening ($i \equiv$ I) or sliding ($i \equiv$ II) modes.

The effect of thickness on the SIFs and mode-mixity is shown in Fig. 7(a)–(c) for a central crack at $R_a = 30$ mm. Non-dimensional mode-I SIF, H_I, (Fig. 7(a)), non-dimensional mode-II SIF, H_II, (Fig. 7(b)) and mode-mixity, $H_\mathrm{II}/H_\mathrm{I}$, (Fig. 7(c)) are plotted against crack-half-arc-angle, β, for beam thicknesses $t = 20, 25, 30$ and 35 mm. Since the same moment is applied to all of the cases, the narrower beams are expected to have higher SIF values for the same size cracks. This is not evident from Fig. 7(a) because of non-dimensionalization done using Eq. (19); which involves the value of σ that decreases with increase in beam thickness for a fixed moment value. The σ values are given in the figure caption. In Fig. 7(a), the non-

dimensional mode-I SIF increases monotonically with crack size for all thicknesses. Again note that overlapping of the graphs for $t = 30$ mm and $t = 35$ mm does not mean equality of the SIF values. Similar trends are seen for the non-dimensionalized mode-II SIF (Fig. 7(b)), however, the change with crack length is more pronounced. In Fig. 7(c), mode-mixity increases with crack size for all thicknesses. For crack half arc angles, β, smaller than 15°, the ratio is the same for all thicknesses (at each β) and remains below 0.15. Afterwards, the graphs for all thicknesses rise to a mode-mixity ratio of 0.3, following each other very closely and in an almost linear trend. It can be observed that in the range of crack sizes considered here, mode-I remains dominant for all thicknesses.

The effect of the crack position along the thickness of the beam ($h_a = (R_a - R_1)/(R_2 - R_1)$) on the SIF and the mode-mixity is shown in Fig. 7(d)–(f) for a 30 mm thick beam ($R_1 = 15$ mm, $R_2 = 45$ mm). Non-dimensional mode-I SIF, H_{I}, non-dimensional mode-II SIF, H_{II}, and mode-mixity, H_{II}/H_I, are plotted as a function of crack-half-arc-angle, β, in Fig. 7(d)–(f), respectively, for different crack positions $h_a = 0.25$, 0.5 and 0.75. For all crack positions, the mode-I SIF increases almost linearly with crack size as shown in Fig. 7(d). It is noted that the mode-I SIF is greater for crack positions closer to the inner radius. In the case of Fig. 7(e), the highest mode-II SIF values belong to the cracks on the center-line ($h_a = 0.5$) and the lowest to $h_a = 0.75$. Therefore $h_a = 0.75$ is the less critical crack position for both of the modes. The mode-mixity again remains below 0.3 (Fig. 7(f)), implying a mode-I dominance for all crack positions along the thickness for the 30 mm thick beam. The mode-mixity is seen to be independent of crack position along the thickness of the beam for smaller crack sizes, as indicated by the overlapping parts of the graphs for $\beta < 15°$.

5. Conclusions

The stress field of an isotropic curved beam with a circumferential crack under pure bending moment was successfully computed by the modified mapping-collocation (MMC) method. The stress correlation technique is then used to calculate opening and sliding mode stress intensity factors for a variety of thicknesses, crack positions and sizes. The solution is found to lose accuracy for crack half angle values of $\beta < 5°$ and $\beta > 30°$; and for non-dimensional beam thickness values, t/R_m, smaller than 0.5 due to numerical difficulties.

The effects of the crack position and the beam thickness on mode-I SIF, mode-II SIF and the mode-mixity are presented as a function of the crack size. As expected, the SIF values for both the modes increase with the crack length. In all cases, the crack tip fields are found to be mode-I dominated. In addition, mode-I SIF values are found to increase as the crack position shifts towards the inner radius of the beam. Furthermore, while the mode-mixity increases with increasing β, it is independent of both the beam thickness and the crack position for small cracks ($\beta < 15°$).

As a semi-analytic approach to treat boundary value problems of 2-D elasticity, the MMC method has advantages such as accuracy and computational efficiency over other purely numerical methods (e.g., finite elements method), especially in dealing with the crack tip linear-elastic singularity. A possible future study would be to apply the method to analyze a circumferential crack in a cylindrically orthotropic curved beam.

Acknowledgment

The authors wish to acknowledge Denizhan Yavas, at the Department of Aerospace Engineering in Middle East Technical University (METU), for the photoelastic test result (Fig. 3b).

References

[1] B. Gozluklu, D. Coker, Modeling of dynamic delamination of L-shaped unidirectional laminated composites, Compos. Struct. 94 (4) (2012) 1430–1442.
[2] O.L. Bowie, D.M. Neal, A modified mapping-collocation technique for accurate calculation of stress intensity factors, Int. J. Fract. Mech. 6 (2) (1970) 199–206.
[3] O.L. Bowie, C.E. Freese, Central crack in plane orthotropic rectangular sheet, Int. J. Fract. Mech. 8 (1) (1972) 49–58.
[4] O.L. Bowie, C.E Freese, Elastic analysis for a radial crack in a circular ring, Eng. Fract. Mech. 4 (1972) 315–321.
[5] P.G. Tracy, Analysis of a radial crack in a circular ring segment, Eng. Fract. Mech. 7 (1975) 253–260.
[6] P.G. Tracy, Elastic analysis of radial cracks emanating from the outer and inner surfaces of a circular ring, Eng. Fract. Mech. 11 (1979) 291–300.
[7] A.T. Zehnder, Fracture mechanics, On-line notes, Sibley School of Mechanical and Aerospace Engineering, Cornell University, 2010.
[8] N.I. Muskhelishvili, Some Basic Problems of the Mathematical Theory of Elasticity, P. Noordhoff, Groningen, 1953.
[9] S.P. Timoshenko, J.N. Goodier, Theory of Elasticity, third ed., McGraw-Hill, New York, 1969.